

Influence of carbon nanoparticles on the polymerization and EMI shielding properties of PU nanocomposite foams

Cite this: *RSC Adv.*, 2014, 4, 7911

M. Mar Bernal,^{*a} Mario Martin-Gallego,^a Isabel Molenberg,^b Isabel Huynen,^b Miguel A. López Manchado^a and Raquel Verdejo^{*a}

Rigid polyurethane (PU) nanocomposite foams filled with multi-walled carbon nanotubes (MWCNTs), functionalized MWCNTs (f-MWCNTs) and functionalized graphene sheets (FGS) were synthesized by reactive foaming to obtain electromagnetic interference (EMI) shielding materials. Our study indicates that the electrical properties of rigid PU nanocomposite foams are strongly dependent on the foaming evolution, cellular structure and density of these materials, which are themselves influenced by the morphology, aspect ratio and surface functionalization of the carbon-based nanofillers. The largest EMI shielding effectiveness was obtained for 0.35 wt% MWCNTs with an electrical conductivity increased of two orders of magnitude ascribed to the formation of a better interconnected network within the systems.

Received 5th October 2013
Accepted 9th January 2014

DOI: 10.1039/c3ra45607b

www.rsc.org/advances

Introduction

Electromagnetic interference (EMI) is defined as the process by which disruptive electromagnetic energy is transmitted from one electronic device to another via radiated or conducted paths or both.¹ Therefore, the function of a shield is to prevent the emissions of the electric and magnetic waves from propagation from one region to another. Nowadays, polymer composites are being studied for EMI shielding applications because of their lightweight, corrosion resistance and ease processability as compared to traditional shields made of metals. In particular, polymer nanocomposite foams filled with carbon nanoparticles are promising systems to use as EMI shielding materials due to the combination of the foam's low density, dielectric constant (ϵ') and thermal conductivity with the unique electrical and mechanical properties of the carbon nanoparticles.^{2–8}

The attenuation performance or effectiveness of EMI shields is considered as a combination of absorption and reflection mechanisms and is normally expressed in decibels (dB). The shielding effectiveness (SE) of common commercial applications is around 20 dB in the X-band region (8–12 GHz) while the target conductivity value is 1 S m^{-1} .⁴ In the literature, these values have mainly been achieved with high contents of nanoparticles in the polymer foams. For example, the target EMI SE value was achieved with the inclusion of 15 wt% of carbon nanofibres (CNFs)³ and 7 wt% nanotubes (CNTs)³ in polystyrene

(PS) foams. Thomassin *et al.*⁴ developed foams of polycaprolactone (PCL) filled with MWCNTs for EMI shielding applications. They achieved shielding efficiencies as high as 60–80 dB with low reflectivity at 2 wt% of MWCNTs (0.25 vol%). Fletcher *et al.*⁵ demonstrated that foaming an elastomer fluorocarbon polymer with MWCNTs reduced the weight of the material by 30% with a minor impact on the EMI properties. Recent studies on foam composites with graphene sheets have been developed with poly(methyl methacrylate) (PMMA)⁷ and polyvinylidene fluoride (PVDF)⁶ foams. These studies obtained an EMI shielding efficiency of around 19 dB with 5 wt% graphene in both PMMA and PVDF foams, attributed to absorption rather than reflection mechanisms. In this work, rigid PU foams filled with different CNPs were prepared in order to enhance the EMI properties of these systems. For this reason, we report the results related to the dispersion and kinetics of polymerization of rigid PU nanocomposite foams which determines their final cellular structure and density that strongly influences the formation of a conductive pathway within these systems.

Experimental

Materials

The polyol blend used for the synthesis with a hydroxyl number of $343.5 \text{ mg KOH g}^{-1}$ was supplied by Alcupol R-4520 (Repsol Química). The isocyanate was a 4,4'-diphenylmethane diisocyanate (MDI), Isocianato H from SynthésiaEspañola S.A. with a viscosity of 300 mPa s^{-1} at $20 \text{ }^\circ\text{C}$ and an isocyanate content of 31 wt%. DABCO 2097 (potassium acetate in diethylene glycol, Air Products) and PC CAT NP 60 (*N,N*-dimethylbenzylamine, Performance Chemicals Handels GmbH) were used as catalysts in the reaction. SILSTAB 2100 (block copolymer of dimethylsiloxane and a

^aInstituto de Ciencia y Tecnología de Polímeros (ICTP-CSIC), C/Juan de la Cierva 3, 28006, Madrid, Spain. E-mail: rverdejo@csic.es; mar.bernal@imdea.org

^bInformation and Communications Technologies, Electronics and Applied Mathematics (ICTEAM), Microwave Laboratory, Université Catholique de Louvain, B-1348 Louvain-la-Neuve, Belgium

polyoxyalkylene, Siltech Corp.) was used as a surfactant, PC TOPA (*N*-[3-(dimethylamino) propyl] tall-oil amide, Performance Chemicals Handels GmbH) was used as a flow improving agent and distilled water was the blowing agent in the reaction.

Multi-walled carbon nanotubes (MWCNTs) were grown by the chemical vapor deposition (CVD) injection method.^{9,10} A 3 wt% ferrocene/toluene solution was injected into a hot quartz tube reactor (760 °C) at 5 ml h⁻¹ under inert atmosphere. These nanotubes were chemically-treated with a 3 : 1 concentrated sulphuric–nitric acid mixture and refluxed at 120 °C for 30 min; then they were filtered and washed with distilled water until neutral pH. The functionalized MWCNTs (f-MWCNTs) were finally dried at 120 °C and stored in a sealed container under vacuum prior to use.

Functionalized graphene sheets (FGS) were produced from the adiabatic expansion¹¹ of graphite oxide at 1000 °C under an inert atmosphere. Graphite oxide was synthesized from natural graphite according to the Brödie method.¹²

Full characterization of the CNP used in this study can be found elsewhere.^{11,13,14}

Preparation of rigid PU nanocomposite foams

Rigid PU foams were prepared following the formulation summarized in Table 1. Two loading fractions of CNPs (MWCNTs, f-MWCNTs and FGS) were selected in this work 0.4 and 0.8 phpp which correspond to 0.17 and 0.35 wt% of the resulting composite foam.

First, a fixed amount of CNPs was added into the polyol. The mixture was initially sonicated for 10 min with an ultrasonication probe (Sonics VibraCell) in a water/ice bath, and was then stirred under high shear at 2400 rpm for 6 h. Subsequently, the surfactant, catalysts and distilled water were added to the polyol/CNP mixture and stirred at 2400 rpm for 3 min. Finally, the isocyanate was added and mixed for 20 s before foaming occurred in an open cylindrical mould.

Characterization

The rheological behavior of the polyol/CNP dispersions was measured using an Anton Paar P-PTD200/ERD Rheological Device. The geometry used was a stainless-steel corrugated parallel plate with a diameter of 20 mm. The gap was fixed to

0.3 mm and a dynamic frequency sweep from 0.01 to 100 rad s⁻¹ at 21 °C was employed. The results were averaged over three different samples. The thermal conductivity of the polyol/CNP dispersions was measured with a KD2 probe (Decagon Devices Inc.). The measurements were carried out at room temperature where no convection was present in the polyol/CNP dispersions. The results were the average of at least six measurements for each sample. The adiabatic temperature rise was used to follow the reaction kinetics of rigid PU nanocomposite foams. The exotherms were determined using a Scanning Vibrating Needle Curemeter (Rapra Technology Ltd.) which measured the temperature of the rising foam. The experimental measurements were carried out by centering a stainless steel type K thermocouple in the middle of the mould where the components were pre-mixed for 20 s. The thermocouple was connected to a computer where the data were registered. The results were the average of at least three diverse foam samples. The experimental error for each set of samples was around 10% ascribed to small-scale laboratory sample preparation and vibrating needle positioning. The structure of the foams was qualitatively examined using a Phillips XL30 environmental scanning electron microscope (ESEM) at 15 kV. Cross-sections of the samples were cryo-fractured perpendicular to the foaming direction and the fracture surface was sputter-coated with gold/palladium. The morphology of the foams was analyzed using the program ImageJ. The density of a cubic sample was measured as the sample weight divided by its volume according to ASTM D 1622-03. The results were the average of at least three different foam materials. The EMI shielding effectiveness was measured with a Wiltron 360B vector network analyzer (VNA) in a frequency range from 8 to 12 GHz. Nanocomposite foams were cut into a rectangle (2.9 cm × 1.07 cm) to fit a steel waveguide sample holder. A full two-port VNA calibration was performed at the beginning of each test sequence to correct systematic measurement errors. The reported results were the average of three tested samples for each foam nanocomposite.

Results and discussion

The study of the rheological behavior of polyol/CNP systems is essential to understand the later foaming process and it provides an effective tool for understanding the dispersion degree in filled polymer systems. The dependence of the complex viscosity with the angular frequency for neat polyol and its filled dispersions at 0.4 and 0.8 phpp of CNPs is shown in Fig. 1.

The rheological behavior of polyol/CNP dispersions can be quantitatively described by the Herschel–Bulkley model (eqn (1)):

$$\eta^* = \frac{\tau_0}{\omega} + k\omega^{n-1} \quad (1)$$

where η^* is the complex viscosity, ω is the angular frequency, τ_0 is the yield stress below which there is no flow, k is the consistency index and n is the flow index which describes the rheological behavior (for $n < 1$ shear-thinning, for $n > 1$ shear thickening and for $n = 1$ Newtonian fluid). Table 2 summarizes

Table 1 Rigid PU formulation

Trade name	Description	phpp ^a
Alcupol R-4520	Polyether polyol	100.00
Isocianato H	Isocyanate	138.38
PC CAT NP60	Amine-catalyst	0.74
DABCO 2097	Catalyst	0.16
SILSTAB 2100	Surfactant	1.58
PC TOPA	Flow improver	3.16
Water	Blowing agent	1.47
CNPs	Nanofiller	0.4
		0.8

^a The amount of each component was based on parts by hundred parts of polyol (phpp).

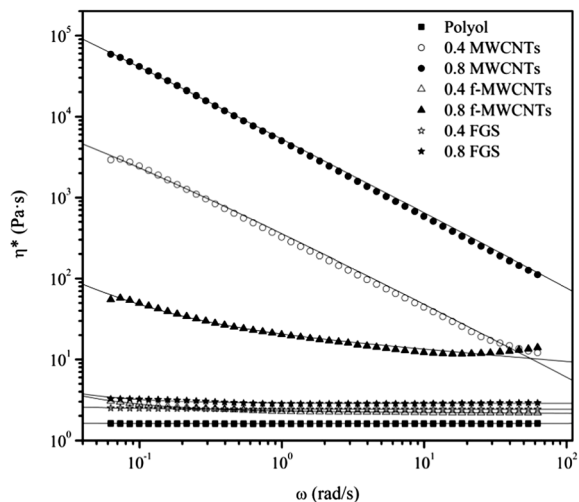


Fig. 1 Variation of the complex viscosity (η^*) as a function of the angular frequency (ω) for polyol/CNP dispersions. The solid lines are the fit to the Herschel–Bulkley model.

the parameters obtained from the fitting of the Herschel–Bulkley model. This model has been previously applied in polyol dispersions for clays¹⁵ and for carbon nanotubes,^{16,17} observing a decrease of the shear-thinning exponent as the concentration of nanoparticles increased in the systems.

The results show a distinctive rheological behavior of the dispersions as a function of the loading amount of CNPs. Neat polyol exhibits the typical behavior of a Newtonian fluid, in which, the viscosity is independent of the frequency. The addition of FGS and low f-MWCNTs loading fractions do not vary the rheological properties of the polyol, showing a flow index value close to 1. However, the dispersions with high loading fractions of f-MWCNTs and in particular, those containing MWCNTs behave as shear-thinning fluids and their complex viscosity η^* increases up to five orders of magnitude compared to the Newtonian fluids. In agreement with previous studies,^{15–17} the shear-thinning exponent of both MWCNTs and f-MWCNTs decreases with increasing loading fractions.

The shear-thinning behavior has widely been observed in polymer nanocomposites^{18,19} and has been ascribed to the development of network structures either through direct interaction of CNPs or polymeric chain bridging between at least two different nanoparticles. The different behavior of the CNPs is related to their different morphology and aspect ratio. Knauert

Table 2 Parameters and the correlation coefficient (r^2) of the Herschel–Bulkley model for the polyol/CNP dispersions

Sample	τ_0 (Pa)	k (Pa s ^{<i>n</i>})	n	r^2
Polyol	≈ 0	1.61	1.00	0.99
0.4 MWCNTs	192.87	181.41	0.57	0.98
0.8 MWCNTs	3740.79	1730.58	0.42	0.98
0.4 f-MWCNTs	0.05	2.25	0.98	0.99
0.8 f-MWCNTs	2.23	18.44	0.83	0.98
0.4 FGS	0.01	2.41	1.00	0.93
0.8 FGS	0.03	2.85	0.99	0.88

*et al.*²⁰ showed that rod-shaped nanoparticles presented the largest complex viscosity and shear-thinning behavior, at any given shear rate, than spherical or sheet-like nanoparticles. They explain this result in terms of the presence of chains that bridge the nanoparticles: MWCNTs readily interact with the polymer chains forming a network of particles interconnected with the matrix; while FGS interact by surface adsorption with the polymer chains and correspondingly have the smallest fraction of bridging chains. Recently, Martin-Gallego *et al.*²¹ described similar results in dispersions of MWCNT and FGS in epoxy resins while Guimont *et al.*²² reported the occurrence of shear-thinning in graphite oxide-PDMS suspensions at concentrations above 2 wt% compared to 0.5 wt% MWCNTs of a previous study.²³ Finally, although both MWCNTs and f-MWCNTs presented a shear-thinning behavior it occurs at different percolation threshold due to the lower aspect ratio of the functionalized nanotubes.¹⁷

The reaction kinetics of the PU, such as rates of polymerization, phase separation, solidification as well as the inherent connectivity between the phases, have a profound effect on the final properties of the system. In this study, three factors have to be considered to establish the effect of CNPs on the reaction kinetics: (i) chain mobility, (ii) CNP functionalization and surface area, and (iii) reaction temperatures. Chain mobility, linked to the system viscosity, has already been reported to control the phase segregation of segmented PU.^{24,25} Hence, large viscosities could result in a slowdown of the reaction kinetics. Meanwhile, large surface area or the presence of oxygen-bearing groups on the CNPs, able of reacting with the isocyanate, could lead to high conversion rates. Finally, due to the highly exothermic nature of the PU reaction, the urethane reaction could be favored by increasing heat transfer.²⁶ Hence, higher values of the thermal conductivities of the initial reactants could enhance the heat transfer in the reaction, and then the reaction rates would be faster.

The thermal conductivities (K) of the polyol dispersions are carried out at room temperature and the results are shown in Table 3.

The thermal conductance in polymer/MWCNT systems is normally assumed to be controlled by a phonon conduction mechanism.^{27,28} The thermal conductivity of CNTs depends on different factors, such as morphology, chirality, diameter and length of the tubes, number of structural defects, specific surface area, as well as on the presence of impurities.^{29–31} All CNPs increase the thermal conductivity of the polyol, being this effect more evident for polyol/MWCNT dispersion, which presents an increase of 50% compared to the neat polyol value.

Table 3 Thermal Conductivity (K) of polyol/CNP dispersions at 0.8 phpp at room temperature

Sample	K (W m ⁻¹ K ⁻¹)
Polyol	0.160 ± 0.001
MWCNTs	0.237 ± 0.004
f-MWCNT	0.188 ± 0.004
FGS	0.170 ± 0.001

Therefore, MWCNTs facilitate an efficient phonon transfer through the inner layers increasing the thermal conductivity of nanofluids.^{32,33} In the case of polyol/f-MWCNTs, the enhancement in K is lower due to the presence of functional groups that disrupt the π -conjugation, decreasing the phonon conduction mechanism and hence lowering the K value. Dispersions of FGS showed even lower values than f-MWCNTs (Table 3). The thermal conductivity of graphene strongly depends on the synthesis method, size of graphene, edge roughness, concentration of defects and the dispersant molecules adsorbed on the surface.³⁴ Hence, the presence of defects and the capacity of adsorption of molecules on their surface, as well as their high specific surface area, reduce the thermal conductivity of polyol/FGS with respect to the dispersions of polyol/MWCNTs. Similar results have been reported in liquid epoxy resins.³²

The extent of conversion in rigid PU nanocomposite foams was followed by an adiabatic temperature rise,^{35–38} which monitors the temperature profile (Fig. 2) during the foaming reaction and hence it enables the evaluation of the extent of the monomer conversions.³⁹ Therefore, the kinetic data on fast bulk polymerizing systems can be calculated as follows.

The energy balance per unit polymer mass can be expressed as:

$$c_p \frac{dT_{\text{exp}}}{dt} = (-\Delta H_r) \frac{dx}{dt} - U(T - T_0) \quad (2)$$

where $c_p = 1.788 \text{ J (g K)}^{-1}$ is the average value of the specific heat taking into account the values given by modern plastics encyclopedia⁴⁰ for cast polyurethane materials, $(-\Delta H_r)$ is the heat evolved per unit polymer mass, U is the global heat transfer coefficient per polymer unit mass, x and T are the conversion and the experimental temperature at a measured time t and T_0 is the temperature at $t = 0$. The adiabatic temperature, T_{ad} , can be obtained from the energy balance for adiabatic conditions and verifies:

$$c_p \frac{dT_{\text{ad}}}{dt} = (-\Delta H_r) \frac{dx}{dt} \quad (3)$$

The adiabatic temperature profile with time of the experimental data is calculated combining eqn (2) and (3) and using the limits $T = T_0$ for $t = 0$ and $T = T_{\text{ad}}$ for the measured time t .

$$T_{\text{ad}} = T_{\text{exp}} + \int_0^t U'(T_{\text{exp}} - T_0) dt \quad (4)$$

where $U' = U/c_p$ is the heat transfer coefficient, obtained by integrating eqn (2) for long times when $dx/dt \rightarrow 0$. Consequently, the conversion of the reaction, x , is given by:

$$x = r \left(\frac{T - T_0}{\Delta T_{\text{ad}}} \right) \quad (5)$$

where r is the stoichiometric ratio of the functional groups, calculated taking into account the formulation data (0.774 in all the experiments) and ΔT_{ad} is the maximum temperature rise. Fig. 3 shows the variation of the conversion x with time for neat and rigid PU nanocomposite foams with 0.35 wt% of CNPs loading fractions and Table 4 reports the average of the ΔT_{ad} in each case. All samples show a similar conversion profile and final degree conversion. However, rigid PU nanocomposite foams have faster conversion rates during the initial stages of the reaction compared to the neat foam (Fig. 3 inset), but no substantial differences are observed among the different CNPs. This similar behavior should be ascribed to a combination of the factors mentioned above. For MWCNTs, the large increase in the thermal conductivity of this system compared to the other two CNPs should have accelerated the reaction,^{26,41} while its high viscosity appears to counteract such effect. In the case of f-MWCNTs and FGS, although the thermal conductivity of these systems is smaller compared to the MWCNTs system, the low viscosities and surface functionalities seem to favor the extent of conversion. Similar effects have been observed using the adiabatic temperature rise method for PU foams with

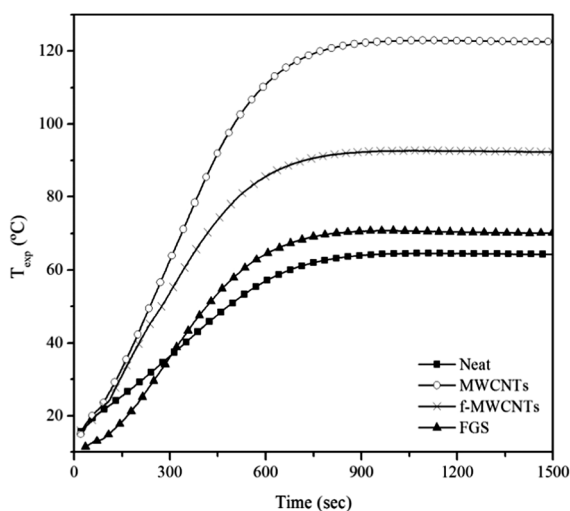


Fig. 2 Variation of the experimental temperature (T_{exp}) with time for rigid polyurethane nanocomposite foams.

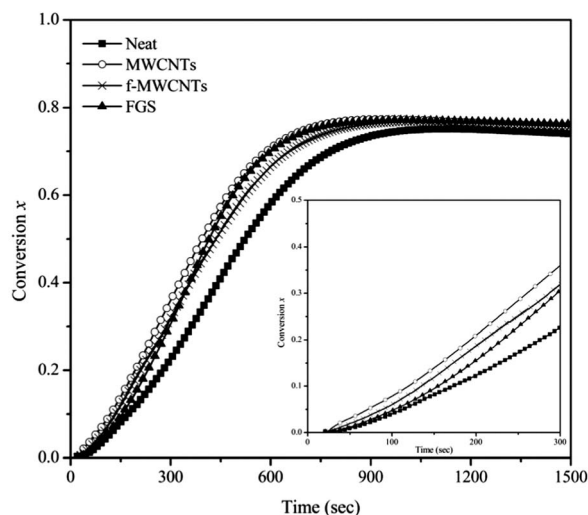


Fig. 3 Variation of the conversion x with time for rigid PU nanocomposite foams.

Table 4 ΔT_{ad} ($^{\circ}\text{C}$) of rigid PU nanocomposite foams from the adiabatic temperature rise measurements

Sample	$\Delta T_{ad, \max}$ ($^{\circ}\text{C}$)
Neat	72.2 ± 5.5
MWCNTs	115.3 ± 5.9
f-MWCNTs	85.5 ± 6.5
FGS	100.2 ± 2.5

montmorillonite (MMT),⁴² and the acceleration was attributed to the surface catalytic effect and the high surface area of the MMT.

The final morphology of foams is determined by the reaction rate which controls the production of gas and the evolution of the fluid rheology.⁴³ Furthermore, it should be considered that in reactive foams two phases govern the foaming dynamics and hence the morphological development: the continuously polymerising liquid matrix and the disperse gas phase.⁴⁴ Both phases are strongly influenced by several parameters (*e.g.* rate of gas production, diffusivity) being surface tension, temperature and viscosity important on the bubble growth, formation and stability. Hence, if temperature increases, both viscosity and surface tension decrease, and then membranes become thinner and in some cases rupture because they cannot support the polymer stresses.^{43–46}

Besides these parameters, in reactive polyurethane nanocomposite foams, two other competing effects influence the cell diameter and should be taken into account: the blowing effect, which increases the cell diameter and the nucleation effect which decreases the cell diameter. The blowing effect is produced by the presence of water on the surface of the nanoparticles. Meanwhile, the nucleation effect depends on the degree of dispersion of nanofillers on the polymer matrix.⁴⁷

The final structure of rigid PU nanocomposite foams is observed by SEM (Fig. 4) and the average cell size is summarized in Table 5. It is widely known that hydrophobic particles can cause instability, producing the rupture of the cells. However, if the particles are well-dispersed in the system, they increase the bulk viscosity and thus can cause an increase of the stability.^{48,49} In addition, the effective stabilization mechanism is higher as the particle size is smaller.⁵⁰ In rigid PU foams filled with MWCNTs a good dispersion of the nanotubes is achieved in the initial system increasing the bulk viscosity which slows down the drainage rate, preventing the rupture of the cells.^{48,49} Hence, even if there is an important increase on the temperature of the reaction during the foaming, the high viscosity is enough to withstand the polymer stresses on the cell walls maintaining the cell structure.^{46,51} Therefore, the clear reduction of the cell diameter (Table 5), as the content of nanoparticles increases, confirms the nucleation effect of MWCNTs on rigid PU foams.

On the other hand, rigid PU foams filled with low contents of f-MWCNTs and FGS show similar cell diameters as 0.17 wt% of MWCNTs. For high contents (0.35 wt%) of f-MWCNTs, the cell diameter is similar to that of neat rigid PU foam. This increase in the cell size as a function of loading fraction suggests that the blowing effect is dominant for these foams due to the

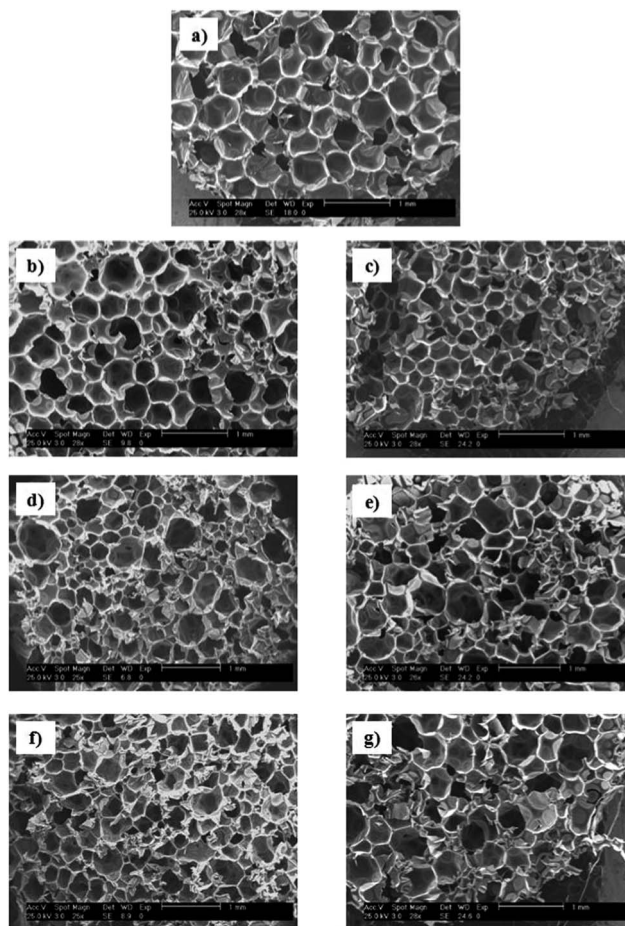


Fig. 4 Representative SEM images of rigid PU nanocomposite foams: (a) neat; (left) 0.17 wt% CNPs (b) MWCNTs, (d) f-MWCNTs, and (f) FGS; (right) 0.35 wt% CNPs (c) MWCNTs, (e) f-MWCNTs, and (g) FGS.

hydrophilic nature of f-MWCNTs. In the case of FGS larger loading fractions (0.35 wt%) results in an increase of the cell diameter although less pronounced than in rigid PU foams with f-MWCNTs, because the content of the hydrophilic groups on the surface of the graphene sheets is lower. In addition, for rigid PU foams filled with high contents of FGS and f-MWCNTs, it can be observed (Fig. 4) a broad distribution of the cell size, which is related to coalescence effects. The lower viscosity of the initial dispersions of f-MWCNTs and FGS causes instability because of the stresses generated in the cell walls by the polymer and the nanoparticles, collapsing the cell structure.

Table 5 Size (μm) and density (kg m^{-3}) of rigid PU nanocomposite foams

Sample	Cell size (μm)	Density (kg m^{-3})
Neat	545 ± 12	82.4 ± 0.4
MWCNTs-0.17 wt%	442 ± 19	75.3 ± 0.6
MWCNTs-0.35 wt%	359 ± 10	70.9 ± 3.5
f-MWCNTs-0.17 wt%	424 ± 48	71.9 ± 2.6
f-MWCNTs-0.35 wt%	533 ± 55	58.2 ± 1.5
FGS-0.17 wt%	427 ± 17	65.1 ± 2.3
FGS-0.35 wt%	476 ± 43	58.2 ± 0.9

Foam density is an important physical property which influences the mechanical properties and hence the final applications of these materials. The densities of rigid PU nanocomposite foams are given in Table 5. It can be observed that as the content of the CNPs increases, the foam density decreases. Fig. 5 shows representative SEM images of rigid PU foams filled with f-MWCNTs and FGS at high magnification where it is observed a good dispersion of the CNPs in the system, being located in the struts and walls of the cellular structure.

The SEM images show thinner cell walls for rigid PU nanocomposite foams, decreasing the foam density. This effect is also observed on the shape of the cell, which can be approximated to regular spheres for unfilled rigid PU foams while in the case of rigid PU nanocomposite foams become polyhedrons.⁵² The low densities for rigid PU foams filled with high contents (0.35 wt%) of f-MWCNTs and FGS are probably caused by the aforementioned instability of the cell structure. In order to confirm these qualitative results, the cell wall thickness and cell density of the rigid PU nanocomposite foams were calculated. The cell wall thickness can be obtained by eqn (6).⁵³

$$\delta = d \left(\frac{1}{\sqrt{1 - \left(\frac{\rho_{\text{foam}}}{\rho_{\text{solid}}}\right)}} - 1 \right) \quad (6)$$

where δ is the cell wall thickness (μm) d is the cell size and $\rho_{\text{foam}}/\rho_{\text{solid}}$ is the ratio of foam density and solid density (the density of the initial liquid system). Fig. 6 shows the variation of the cell wall thickness for the different nanocomposite foams at the different wt% of nanoparticles. As can be observed, the cells become thinner as the content of carbon nanoparticles increases on the samples confirming the above mentioned discussions. Furthermore the cell density of the nanocomposite foams were calculated taking into account eqn (7):⁵⁴

$$N_{\text{cell}} = \frac{6}{\pi d^3} \left(\frac{\rho_{\text{foam}}}{\rho_{\text{solid}}} - 1 \right) \quad (7)$$

where N_{cell} is defined as the number of cells per unit of volume of the solid materials ($n \text{ cm}^{-3}$). Fig. 7 shows the results obtained based on eqn (7). The cell density increases as the content of carbon nanoparticles increases on the PU nanocomposite foams due to the nucleation effect. However, for higher contents of f-MWCNTs and FGS a dramatic decrease of the cell density can be observed. This change on the evolution of the cell density for these two types of carbon nanoparticles corroborated the observed instability of their cellular structure by SEM images and the aforementioned discussions.

The EMI shielding effectiveness (SE) of rigid PU nanocomposite foams was measured in the X-band frequency region (8–12 GHz). The measured shielding effectiveness (SE) is defined as the ratio between the incident power (P_{in}) and the

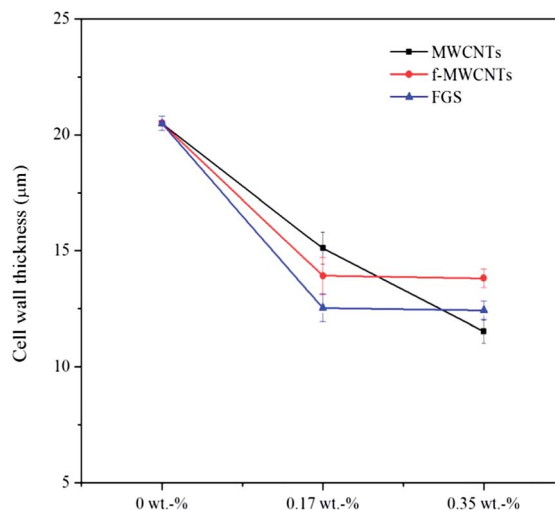


Fig. 6 Cell wall thickness (μm) of rigid PU nanocomposite foams at different wt%.

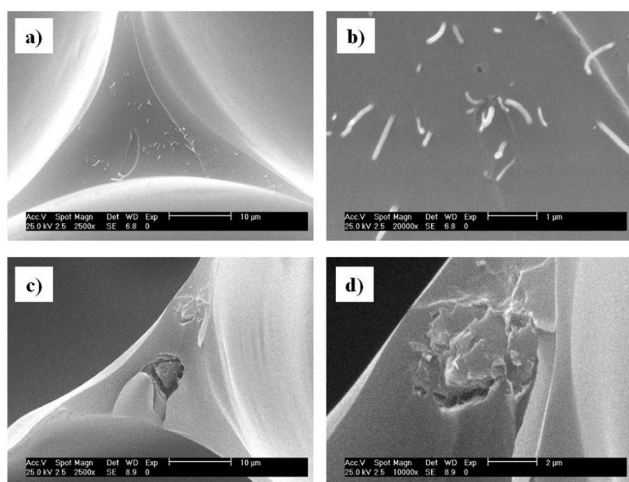


Fig. 5 Representative SEM images at high magnification of rigid PU foam filled with f-MWCNTs (a) 10 μm and (b) 1 μm and FGS (c) 10 μm and (d) 2 μm .

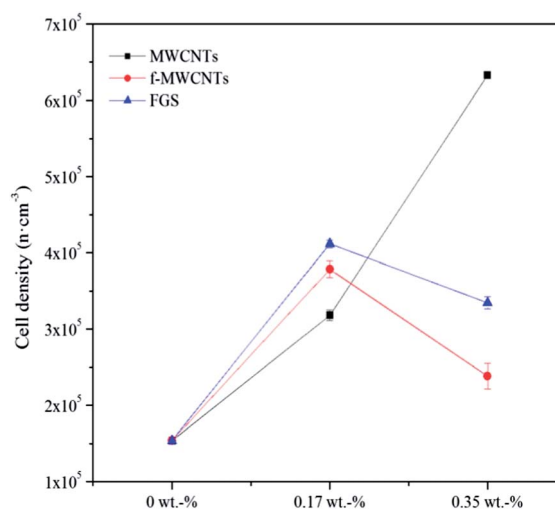


Fig. 7 Cell density ($n \text{ cm}^{-3}$) of rigid PU nanocomposite foams at different wt%.

power transmitted through a shielding material (P_{out}). The SE is expressed in decibels (dB): $SE = 10 \log(P_{in}/P_{out})$. Fig. 8a shows the comparison of the specific EMI SE for high loading contents of CNPs normalized by the density of the nanocomposite foams. As it is expected, the presence of CNPs increases the values of the specific EMI shielding effectiveness and it can be observed that this value is almost independent of the frequency on the studied frequency region. While the average value for neat rigid PU foam was approximately $4 \text{ dB cm}^3 \text{ g}^{-1}$, the inclusion of 0.35 wt% of f-MWCNTs and FGS enhances this value to around 12.5 and $9.8 \text{ dB cm}^3 \text{ g}^{-1}$, respectively. On the other hand, for MWCNT sample the specific EMI shielding effectiveness was more frequency dependent and the maximum value achieved for 0.35 wt% at 12 GHz was around $38.7 \text{ dB cm}^3 \text{ g}^{-1}$. The increase in EMI shielding effectiveness is attributed to an increase in conductivity of the nanocomposite foams (Fig. 5b). The conductivity increases by two orders of magnitude for foams with 0.35 wt% of MWCNTs and by one order for f-MWCNTs and FGS compared to the neat foam. Hence, raw MWCNTs form a better conductive network than f-MWCNTs and FGS in rigid PU nanocomposite foams. As a result, the explanation to the observed results is the combination of two different aspects: (i) the morphology and functionalization of carbon nanoparticles and (ii) the cellular structure of the final

foams. Foams with f-MWCNTs presented lower values of EMI shielding and conductivity than the ones with MWCNTs, which is ascribed not only to the lower aspect ratio of f-MWCNTs but also to the oxygen-bearing groups of their surface, creating defects on the crystalline structure of the carbon nanotubes and hence reducing the number of π -electrons. The same effect was observed on foams filled with FGS where the presence of functional groups on their surface prevents the high electronic transport of π -electrons.²¹ On the other hand, the cellular structure of the final foams plays a key role on the EMI shielding effectiveness of these polymer materials. Rigid PU nanocomposite foams with higher density and less collapsed structure favors the formation of a better conductive pathway due to an increase of the number of contacts between the nanoparticles,^{52,55} as it is observed for foams filled with MWCNTs. Furthermore, it should be highlighted that the EMI SE value obtained for rigid PU foams with only 0.35 wt% of MWCNTs, if the normalization by the density is not taking into account, is 27 dB which is higher than the targeted value for commercial applications, 20 dB. In the literature, similar values were obtained for higher contents of nanoparticles in the final polymer foam, thus these rigid PU foams could be considered as promising materials for EMI shielding applications.

Conclusions

The influence of the morphology, functionality and aspect ratio of carbon nanofillers on the formation and properties of rigid PU foams was evaluated. An increase of the initial viscosity and thermal conductivity of the polyol/CNP dispersions played a key role on the extent of conversion of the reaction and, hence, it affected the cellular structure and density of the resultant nanocomposite foams. EMI shielding effectiveness of rigid PU foams was sensibly increased by the addition of carbon nanofillers. MWCNTs were the most effective filler enhancing the EMI shielding effectiveness by two orders of magnitude due to the formation of a better interconnected network within the system.

Acknowledgements

The authors gratefully acknowledge the financial support of the Spanish Ministry of Science and Innovation (MICINN) through MAT 2010-18749 and the 7th Framework Program of E.U. through HARCANA (NMP3-LA-2008-213277). MMB and MMG also acknowledge the FPI and JAE-Pre programs from MICINN and CSIC, respectively. I.H. is Research Director of the Research Science Foundation (FRS-FNRS), Belgium. All authors acknowledge the department of Applied Physics I of the Faculty of Physics in the Complutense University in Madrid for the thermal conductivity analysis.

References

- 1 C. X. Tong, *Advanced materials and design for electromagnetic interference shielding*, CRC Press, Boca Raton, FL, 2009.

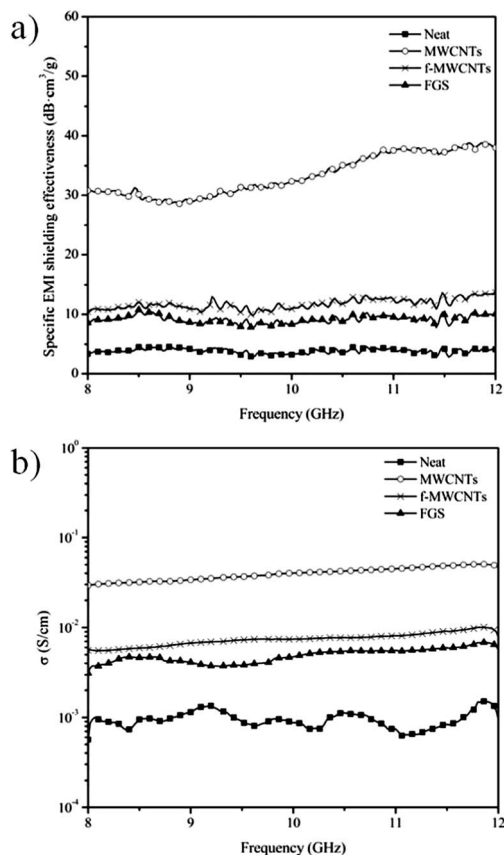


Fig. 8 (a) Specific EMI shielding effectiveness and (b) electrical conductivity (σ) of rigid PU nanocomposite foams at 0.35 wt% CNPs as a function of frequency.

- 2 Y. Yang, M. C. Gupta, K. L. Dudley and R. W. Lawrence, *Nano Lett.*, 2005, **5**, 2131–2134.
- 3 Y. Yang, M. C. Gupta, K. L. Dudley and R. W. Lawrence, *Adv. Mater.*, 2005, **17**, 1999–2003.
- 4 J.-M. Thomassin, C. Pagnoulle, L. Bednarz, I. Huynen, R. Jerome and C. Detrembleur, *J. Mater. Chem.*, 2008, **18**, 792–796.
- 5 A. Fletcher, M. C. Gupta, K. L. Dudley and E. Vedeler, *Compos. Sci. Technol.*, 2010, **70**, 953–958.
- 6 V. Eswaraiah, V. Sankaranarayanan and S. Ramaprabhu, *Macromol. Mater. Eng.*, 2011, **296**, 894–898.
- 7 H. B. Zhang, Q. Yan, W. G. Zheng, Z. He and Z. Z. Yu, *ACS Appl. Mater. Interfaces*, 2011, **3**, 918–924.
- 8 J. M. Thomassin, D. Vuluga, M. Alexandre, C. Jérôme, I. Molenberg, I. Huynen and C. Detrembleur, *Polymer*, 2012, **53**, 169–174.
- 9 C. Singh, M. S. Shaffer and A. H. Windle, *Carbon*, 2003, **41**, 359–368.
- 10 R. Verdejo, S. Lamoriniere, B. Cottam, A. Bismarck and M. Shaffer, *Chem. Commun.*, 2007, 513–515.
- 11 R. Verdejo, F. Barroso-Bujans, M. A. Rodriguez-Perez, J. A. de Saja and M. A. Lopez-Manchado, *J. Mater. Chem.*, 2008, **18**, 2221–2226.
- 12 B. C. Brödie, *Philos. Trans. R. Soc. London*, 1859, **149**, 249–259.
- 13 M. M. Bernal, M. Martin-Gallego, L. J. Romasanta, A.-C. Mortamet, M. A. López-Manchado, A. J. Ryan and R. Verdejo, *Polymer*, 2012, **53**, 4025–4032.
- 14 M. Hernandez, M. D. Bernal, R. Verdejo, T. A. Ezquerro and M. A. Lopez-Manchado, *Compos. Sci. Technol.*, 2012, **73**, 40–46.
- 15 H. S. Xia and M. Song, *Polym. Int.*, 2006, **55**, 229–235.
- 16 H. S. Xia and M. Song, *Soft Matter*, 2005, **1**, 386–394.
- 17 M. M. Bernal, M. A. Lopez-Manchado and R. Verdejo, *Macromol. Chem. Phys.*, 2011, **212**, 971–979.
- 18 D. W. Litchfield and D. G. Baird, in *Rheology Reviews 2006*, The British Society of Rheology, 2006, pp. 1–60.
- 19 S. Bhattacharya, R. K. Gupta and S. Bhattacharya, in *Polymer Nanocomposites Handbook*, ed. R. K. Gupta, K.-J. Kim and E. Kennel, CRC Press, Boca Raton, Florida, USA, 2009, pp. 151–204.
- 20 S. T. Knauert, J. F. Douglas and F. W. Starr, *J. Polym. Sci., Part B: Polym. Phys.*, 2007, **45**, 1882–1897.
- 21 M. Martin-Gallego, M. M. Bernal, M. Hernandez, R. Verdejo and M. A. Lopez-Manchado, *Eur. Polym. J.*, 2013, **49**, 1347–1353.
- 22 A. Guimont, E. Beyou, G. G. Martin, P. Sonntag and P. Cassagnau, *Macromolecules*, 2011, **44**, 3893–3900.
- 23 A. Beigbeder, M. Linares, M. Devalckenaere, P. Degee, M. Claes, D. Beljonne, R. Lazzaroni and P. Dubois, *Adv. Mater.*, 2008, **20**, 1003–1007.
- 24 Y. Li, Z. Ren, M. Zhao, H. Yang and B. Chu, *Macromolecules*, 1993, **26**, 612–622.
- 25 Y. Camberlin and J. P. Pascault, *J. Polym. Sci., Part B: Polym. Phys.*, 1984, **22**, 1835–1844.
- 26 G. G. Viola and W. R. Schmeal, *Polym. Eng. Sci.*, 1994, **34**, 1173–1186.
- 27 J. Hone, M. Whitney, C. Piskoti and A. Zettl, *Phys. Rev. B: Condens. Matter Mater. Phys.*, 1999, **59**, R2514–R2516.
- 28 T. Yamamoto, S. Watanabe and K. Watanabe, *Phys. Rev. Lett.*, 2004, **92**.
- 29 T. Maeda and C. Horie, *Phys. B*, 1999, **263**, 479–481.
- 30 A. Kasuya, Y. Saito, Y. Sasaki, M. Fukushima, T. Maeda, C. Horie and Y. Nishina, *Mater. Sci. Eng., A*, 1996, **217**, 46–47.
- 31 V. N. Popov, *Carbon*, 2004, **42**, 991–995.
- 32 M. Martin-Gallego, R. Verdejo, M. Khayet, J. M. Ortiz de Zarate, M. Essalhi and M. A. Lopez-Manchado, *Nanoscale Res. Lett.*, 2011, **6**.
- 33 Z. D. Han and A. Fina, *Prog. Polym. Sci.*, 2011, **36**, 914–944.
- 34 W. Yu, H. Xie, X. Wang and X. Wang, *Phys. Lett. A*, 2011, **375**, 1323–1328.
- 35 J. Jordan, K. I. Jacob, R. Tannenbaum, M. A. Sharaf and I. Jasiuk, *Mater. Sci. Eng., A*, 2005, **393**, 1–11.
- 36 M. Modesti, V. Adriani and F. Simioni, *Polym. Eng. Sci.*, 2000, **40**, 2046–2057.
- 37 M. Moniruzzaman and K. I. Winey, *Macromolecules*, 2006, **39**, 5194–5205.
- 38 S. Tan, T. Abraham, D. Ference and C. W. Macosko, *Polymer*, 2011, **52**, 2840–2846.
- 39 M. J. Elwell, *Thermochim. Acta*, 1995, **269**, 145–157.
- 40 J. Agranoff, *Modern plastics encyclopedia, 1985-1986*, McGraw-Hill, 1985.
- 41 E. Broyer, C. W. Macosko, F. E. Critchfield and L. F. Lawler, *Polym. Eng. Sci.*, 1978, **18**, 382–387.
- 42 A. N. Wilkinson, N. H. Fithriyah, J. L. Stanford and D. Suckley, *Macromol. Symp.*, 2007, **256**, 65–72.
- 43 S. L. Everitt, O. G. Harlen, H. J. Wilson and D. J. Read, *J. Non-Newtonian Fluid Mech.*, 2003, **114**, 83–107.
- 44 G. Harikrishnan, T. U. Patro, A. R. Unni and D. V. Khakhar, *Soft Matter*, 2011, **7**, 6801–6804.
- 45 D. Klempner and V. Sendjarevic, *Handbook of polymeric foams and foam technology*, Hanser Publishers, Munich, 2004.
- 46 R. Verdejo, R. Stampfli, M. Alvarez-Lainez, S. Mourad, M. A. Rodriguez-Perez, P. A. Bruhwiler and M. Shaffer, *Compos. Sci. Technol.*, 2009, **69**, 1564–1569.
- 47 O. M. Istrate and B. Chen, *Soft Matter*, 2011, **7**, 1840–1848.
- 48 S. T. Lee and N. S. Ramesh, *Polymeric foams: mechanisms and materials*, CRC Press LLC, Boca Raton, Florida, USA, 2004.
- 49 R. J. Pugh, *Adv. Colloid Interface Sci.*, 1996, **64**, 67–142.
- 50 F.-Q. Tang, Z. Xiao, J.-A. Tang and L. Jiang, *J. Colloid Interface Sci.*, 1989, **131**, 498–502.
- 51 T. Kostakis, R. Ettelaie and B. S. Murray, *Langmuir*, 2006, **22**, 1273–1280.
- 52 X.-B. Xu, Z.-M. Li, L. Shi, X.-C. Bian and Z.-D. Xiang, *Small*, 2007, **3**, 408–411.
- 53 M.-P. Tran, C. Detrembleur, M. Alexandre, C. Jerome and J.-M. Thomassin, *Polymer*, 2013, **54**, 3261–3270.
- 54 S. Pardo-Alonso, E. Solorzano, S. Estravis, M. A. Rodriguez-Perez and J. A. de Saja, *Soft Matter*, 2012, **8**, 11262–11270.
- 55 L. Chen, D. Rende, L. S. Schadler and R. Ozisik, *J. Mater. Chem. A*, 2013, **1**, 3837–3850.